Structural Model for Oxygen Permeability of a Liquid Crystalline Polymer

Y. S. Hu, D. A. Schiraldi, A. Hiltner,* and E. Baer

Department of Macromolecular Science and Center for Applied Polymer Research, Case Western Reserve University, Cleveland, Ohio 44106-7202

Received January 28, 2003

ABSTRACT: This study examined the solid-state structure and oxygen transport properties of smectic poly(diethylene glycol 4,4′-bibenzoate) (PDEGBB). The polymer was quenched from the isotropic melt to the smectic liquid crystalline glass and subsequently isothermally crystallized by heating above the glass transition temperature. Crystallized PDEGBB was characterized by thermal analysis and X-ray diffraction. Gas transport properties were characterized by oxygen permeability, diffusivity, and solubility at 1 atm. Oxygen solubility decreased linearly with crystallinity as determined by the heat of melting. This result supported a simple two-phase model of impermeable crystals dispersed in a permeable liquid crystalline (LC) glass. Extrapolation to zero solubility gave a crystal density of 1.371 g cm^{-3}; the corresponding heat of the crystal-to-smectic transition was 10.1 kJ mol^{-1}. The solid-state morphology was examined by atomic force microscopy. A hierarchical structure was proposed for the smectic LC polymer in which mesogens organized into smectic layers, stacks of layers formed wavy lamellae, and assemblies of lamellae defined domains. The lamellar morphology remained after crystallization. It was suggested that crystallized PDEGBB possessed small crystals of low aspect ratio dispersed in the permeable LC phase. This model provided the structural basis for describing oxygen permeability in terms of the generalized Maxwell equation for spherical particles.

Introduction

Aromatic liquid crystalline polyesters have remarkably low gas permeability. In an effort to exploit this characteristic, blending liquid crystalline polymers (LCPs) with thermoplastics has been investigated as a method for improving barrier properties.[1−3] The extraordinarily low gas permeability of LCPs stems mainly from low solubility rather than from low diffusivity.[4−6] Two models were put forward to explain the low solubility.[7−10] One considers the liquid crystal as being intermediate between the impermeable 3-dimensional crystal and the permeable amorphous glass; hence, LC order naturally leads to inherently low gas solubility. The other considers the liquid crystal, like the 3-dimensional crystal, as being impermeable. In this model only domain boundaries and other defect regions are accessible to penetrant molecules. Most of the speculation is based on results for nematic Vectra and Vectra-like poly(*p*-hydroxybenzoate-*co*-*p*-hydroxynaphthoate) copolymers, and it is generally agreed that the existing data are not sufficient to definitively support either model.[4−8,11]

Determining where the mesophase lies between the amorphous glass and the 3-dimensional crystal in terms of gas permeability is a critical step in understanding the gas transport properties in LCPs. In contrast to 3-dimensional crystals, polymeric nematic and smectic mesophases undergo a glasslike transition as well as sub-T_g secondary relaxations, indicating that even at low temperatures these phases support a relatively dynamic environment.[12−15] In addition, the density of most polymeric mesophases, although higher than that of an isotropic glass, is nonetheless much lower than that of a crystalline solid.[16,17] Thus, the possibility that the mesophase is permeable to some extent cannot be immediately dismissed.

* Corresponding author: e-mail pah6@cwru.edu.

The two-phase transport model has been exceptionally useful for describing the effect of crystallization on oxygen transport of non-LC aromatic polyesters particularly when used in conjunction with structural models derived from morphological observations. Examples include poly(ethylene terephthalate) (PET),[18] poly(ethylene naphthalate) (PEN),[19] and a copolymer of ethylene terephthalate and ethylene bibenzoate (PETBB55).[20] Appearance of compact spherulites with sharp boundaries provides a structural model of PET and PEN that identifies a permeable amorphous matrix containing dispersed spherulites of lower permeability. The model is the structural basis for describing oxygen permeability in terms of the generalized Maxwell equation. In contrast, melt-crystallized PETBB55 has poorly organized spherulites with irregular boundaries. Gas transport through this structure requires a different modeling approach. Consideration of a dispersion of impermeable platelets in a permeable matrix, modeled by the Cussler equation, proved successful.

These studies established gas transport as an effective structural probe of crystalline polymers. It appears timely to extend this approach to liquid crystalline polymers. The complex phase transitions and morphologies typical of LCPs present a challenge to modeling efforts. Linear alkylene bibenzoates constitute a well-characterized family of smectic LCPs.[21−23] Poly(diethylene glycol 4,4′-bibenzoate) (PDEGBB) was chosen for study because the solid state can be systematically varied from an LC glass to a crystallized LC glass. The present study tests the permeability of the smectic phase by examining the effect of cold crystallization on oxygen transport properties. The morphology of PDEGBB is examined in order to develop a structural model for oxygen transport.

10.1021/ma0300746 CCC: $25.00
Published on Web 04/15/2003

Table 1. Physical Properties and Oxygen Barrier of PDEGBB

classification	sample	density (g cm^{-3})	ΔC_p (J g^{-1} °C^{-1})	T_g (°C)	ΔH_{X-S} (J g^{-1})	P [cm^3 (STP) cm m^{-2} atm^{-1} day^{-1}]	D ($\times 10^{-13}$ m^2 s^{-1})	S [cm^3 (STP) cm^{-3} atm^{-1}]	ϕ_c
LC glass	Q	1.3201 ± 0.0006	0.258	42		0.0318 ± 0.0004	2.6 ± 0.1	0.0142 ± 0.0002	
	SC155	1.3309 ± 0.0017	0.251	42		0.0267 ± 0.0005	2.7 ± 0.1	0.0114 ± 0.0003	
	A155-8h	1.3299 ± 0.0009	0.250	42		0.0266 ± 0.0008	2.6 ± 0.1	0.0118 ± 0.0002	
cold-crystallized LC glass	A80-0.5h	1.3243 ± 0.0024	0.210	43	1.9 ± 0.1	0.0290 ± 0.0004	2.5 ± 0.1	0.0135 ± 0.0001	0.05
	A65-6h	1.3260 ± 0.0010	0.200	44	2.2 ± 0.3	0.0280 ± 0.0003	2.4 ± 0.1	0.0134 ± 0.0004	0.06
	A80-2h	1.3305 ± 0.0010	0.150	45	5.6 ± 0.3	0.0237 ± 0.0005	2.5 ± 0.1	0.0114 ± 0.0004	0.20
	A65-90h	1.3359 ± 0.0017	0.110	48	8.7 ± 0.7	0.0206 ± 0.0002	2.4 ± 0.1	0.0099 ± 0.0001	0.30
	A80-26h	1.3373 ± 0.0015	0.081	50	10.2 ± 0.4	0.0185 ± 0.0002	2.2 ± 0.1	0.0097 ± 0.0003	0.32
	A80-72h	1.3412 ± 0.0017	0.066	52	14.0 ± 0.7	0.0154 ± 0.0003	2.1 ± 0.1	0.0085 ± 0.0001	0.40

Materials and Methods

Poly(diethylene glycol 4,4′-bibenzoate) (PDEGBB) was provided by KoSa (Spartanburg, SC) in the form of extruded pellets. The chemical structure of PDEGBB is

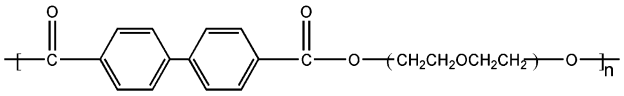

The intrinsic viscosity of the PDEGBB pellets was 0.61 dL g^{-1}, measured at 25 °C in 1% (w/w) dichloroacetic acid solution. Poly(trimethylene terephthalate) (PTT) pellets were also provided by KoSa with an intrinsic viscosity of 0.79 dL g^{-1} measured in the same method as PDEGBB.

The pellets were dried in vacuo at 80 °C for 24 h prior to molding. Films 180−200 μm thick were obtained by compression-molding the pellets between Teflon-coated aluminum sheets in a press at 250 °C (40 °C above the clearing point). The platens were heated in the press for 3 min with repeated application and release of pressure to remove air bubbles and held at 309 psi (2.1 MPa) for an additional 3 min. The polymer could not be quenched to the amorphous state due to the extremely rapid isotropic to liquid crystalline transition. Quenched LC films were obtained by plunging the isotropic melt into ice water. Some of the quenched films were subsequently annealed at constant temperature (65, 80, or 155 °C) for a period of time and quenched in ice water. The annealed films are identified by the letter A followed by the annealing temperature and time (Table 1). Another film, identified as SC 155, was slowly cooled in the press at approximately 2 °C min^{-1} from 250 to 155 °C and quenched into ice water.

Density was measured at 23 °C with a density gradient column constructed from an aqueous solution of calcium nitrate in accordance with ASTM-D 1505 method B. The column was calibrated with glass floats of known density. Small pieces of film (~25 mm^2) were placed in the column and allowed to equilibrate for 30 min before the measurements were taken.

Thermal analysis was conducted with a Perkin-Elmer DSC-7 calibrated with indium and tin under nitrogen. Heating and cooling scans were performed at 10 °C min^{-1} over the temperature range from 0 to 280 °C.

Relaxation behavior was measured in a dynamic mechanical thermal analyzer (DMTA) Mk II unit from Polymer Laboratories (Amherst, MA) operated in the tensile mode with a frequency of 1 Hz and heating rate of 3 °C min^{-1}.

Wide-angle X-ray diffraction (WAXD) powder patterns were obtained at ambient temperature with a Philips diffractometer in the transmission mode using a slit angle of 1/12°. An oriented film was prepared by cold drawing the quenched film at 65 °C and heat setting it at 155 °C for 6 h under tension. The X-ray fiber pattern was recorded using a Statton camera and Ni-filtered Cu Kα radiation calibrated with calcium fluoride.

Conformational composition was determined by photoacoustic Fourier transform infrared (FTIR) spectroscopy. Spectra were collected at ambient temperature with a Nicolet 870 FTIR spectrometer using a MTEC model 200 photoacoustic cell. Specimens were cut from the molded films and dried overnight in vacuo at ambient temperature to remove moisture. Spectroscopic determination of the fraction of trans conformations is described elsewhere.[24]

Free surfaces were prepared for atomic force microscopy (AFM). Small pieces of the pellet were sandwiched between clean glass cover slides, heated into the isotropic state (about 230 °C) on the hot stage of an optical microscope, and lightly pressed to spread out the melted polymer. After the specimen was removed from the hot stage and cooled to ambient temperature, one of the cover slides was peeled off to create a free surface. The specimen with the free surface was vacuum-dried, remelted under nitrogen, and subjected to a thermal history that mimicked the compression-molded films, i.e., quenched, annealed, or slowly cooled. The free surfaces were etched with 40 wt % aqueous methylamine solution at 23 °C using the procedures of Organ et al.[25] The etched specimens were washed with deionized water and methanol. The etching time was varied from 1 to 48 h. Initially, the specimens were about 35−50 μm in thickness. Etching for 48 h removed material from the surface to a depth of about 200−400 nm. The etched surfaces were examined by AFM; the images were obtained in air at ambient conditions using the Nanoscope IIIa MultiMode head from Digital Instruments (Santa Barbara, CA). Experiments were conducted in the tapping mode using Si probes with 50 N m^{-1} spring constant and resonance frequencies in the range 284−362 kHz. The tip had a radius of 10 nm. Height and phase images were recorded simultaneously.

The oxygen flux $J(t)$ at 0% relative humidity, 1 atm pressure, and 23 °C was measured with a MOCON OX-TRAN 2/20. Specimens were carefully conditioned as described previously[18] in order to obtain the non-steady-state oxygen flux from which the diffusivity D was determined. To obtain the diffusivity D and to accurately determine the permeability P, the data were fit to the solution of Fick's second law with appropriate boundary conditions[18]

$$J(t) = \frac{Pp}{l}\left[1 + 2\sum_{n=1}^{\infty}(-1)^n \exp\left(-\frac{D\pi^2 n^2 t}{l^2}\right)\right] \qquad (1)$$

As indicated previously,[18] the error in determining the two fitting parameters, P/l and D/l^2, was estimated not to exceed 2%. The low sensitivity of the flux to thickness variation within 30% was demonstrated previously.[18] Therefore, the accuracy of P and D was determined mainly by the accuracy of the average thickness measurement. The average thickness l of each specimen was determined as $l = W(A\rho)^{-1}$, where W is the sample weight, A is the sample area, and ρ is the density. All the samples were stored in the freezer, and all the analyses were accomplished within 4 weeks of preparation in order to avoid possible aging effects.

Results and Discussion

Thermal Transitions. The thermograms in Figure 1 were obtained by cooling PDEGBB from 280 to 0 °C at a rate of 10 °C min^{-1} and subsequently heating it at the same rate. The cooling curve contained a sharp exothermic peak at 186 °C followed by the glass transi-

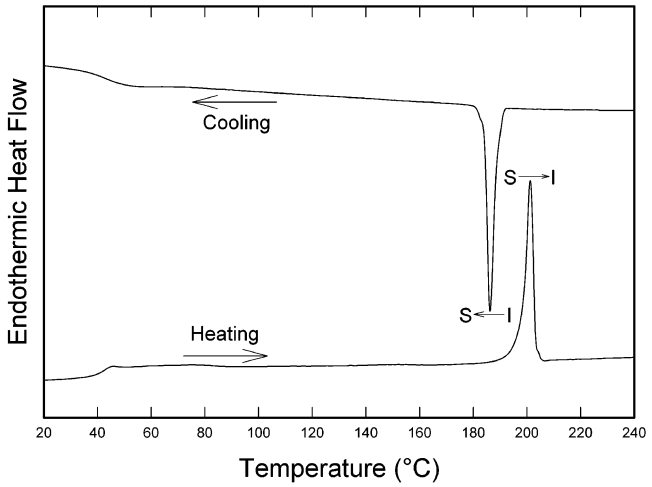

Figure 1. Thermograms of PDEGBB cooled from the isotropic melt to the LC glass and reheated at 10 °C min^{-1}.

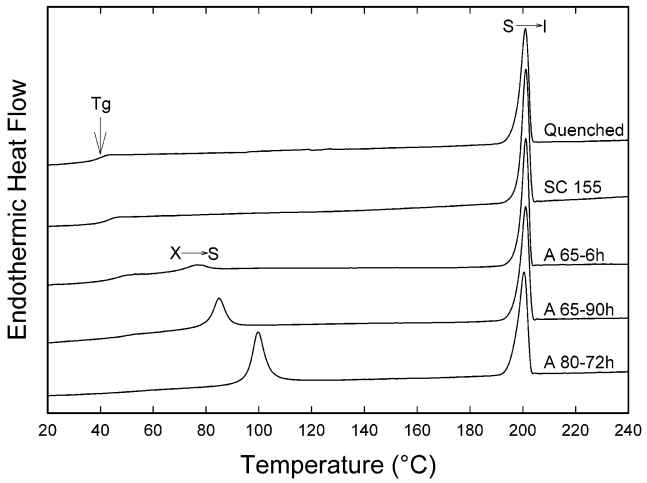

Figure 2. Thermograms of PDEGBB with various thermal histories.

tion at 42 °C. The heating curve showed a sharp endothermic peak at 201 °C. The small supercooling suggested that the transition was liquid crystalline in nature, probably the smectic-to-isotropic (S−I) transition. The absence of crystallization and melting peaks categorized PDEGBB as an LC glass.

The heating thermogram of compression-molded PDEGBB that had been quenched from the melt exhibited the glass transition and S−I transition as in Figure 1. The heating thermogram of PDEGBB that had been slowly cooled from the isotropic melt through the I−S transition to 155 °C and then quenched was also the same, although the density increased from 1.3201 g cm^{-3} for quenched PDEGBB to 1.3309 g cm^{-1}, suggesting that slow cooling produced an LC glass with slightly better order than quenching directly from the isotropic melt. Annealing quenched PDEGBB at 155 °C, just below the S−I transition, also increased the density of the glass but did not alter the heating thermogram. Regardless of the thermal history, the enthalpy of the S−I transition ΔH_{S-I} was 17.4 J g^{-1}.

Annealing quenched PDEGBB at a temperature above the T_g but well below the S−I transition produced the thermograms in Figure 2. The S−I peak was preceded by a new endothermic peak at 75−100 °C. The accompanying shift in the glass transition to higher temperature and smaller ΔC_p was consistent with

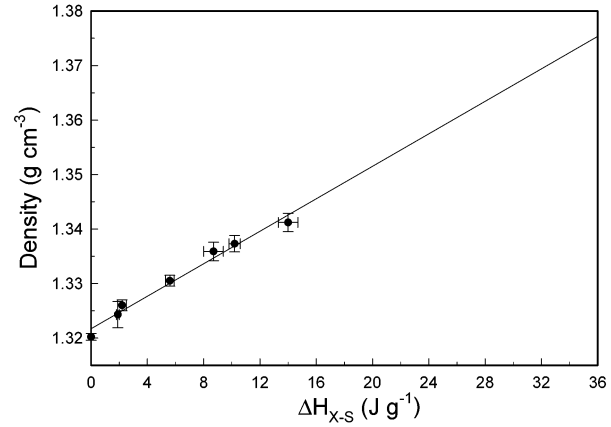

Figure 3. Relationship between density and enthalpy of the crystal to smectic (X−S) transition.

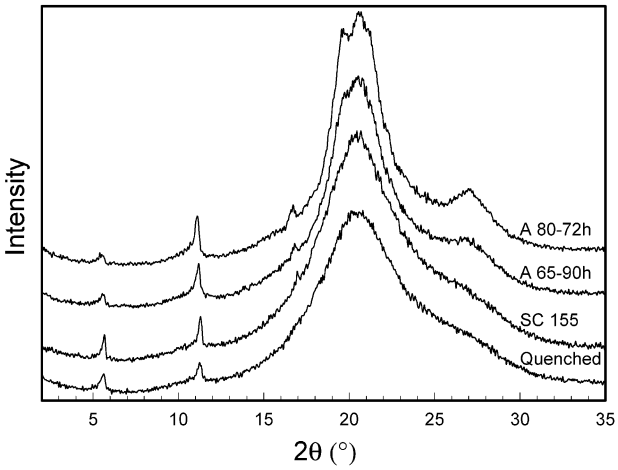

Figure 4. WAXD scans of PDEGBB films.

development of 3-dimensional crystalline order. Accordingly, the new endotherm was attributed to the crystal to smectic (X−S) transition. Even after prolonged annealing, the melting enthalpy was only 14.0 J g^{-1}. Such a low value of ΔH_{X-S} seems to be characteristic of the crystal-to-smectic transition for LC poly(bibenzoates) with an odd number of carbon atoms in the spacer backbone.[26,27] An increase in density accompanied crystallization; the data defined a single linear relationship between density and ΔH_{X-S} regardless of the crystallization temperature (Figure 3).

Wide-Angle X-ray Diffraction. The WAXD pattern of quenched films exhibited a sharp peak at $2\theta = 5.65°$ (15.6 Å), corresponding to the spacing of the smectic layers (Figure 4). This spacing was less than the calculated length of the fully extended repeat unit of 18.2 Å. It was frequently observed with smectic LCPs that the layer spacing measured from WAXD was less than the fully extended length; this dfference was attributed to the presence of some gauche or eclipsed conformations of the spacer.[27−30] Infrared analysis confirmed that the spacer was not fully extended in PDEGBB.[24] The trans fraction was found to be 0.79, which allowed for a significant fraction of non-trans conformations. A broad reflection centered at 20.5° (4.33 Å) was attributed to lateral packing of the mesogens.

The diffraction pattern of the stretched film revealed the orientation of the mesogens in the smectic layers (Figure 5). The layer reflections formed arcs on the meridian with the same spacing as in the quenched film, whereas the broad reflection at 20.5° was split into two

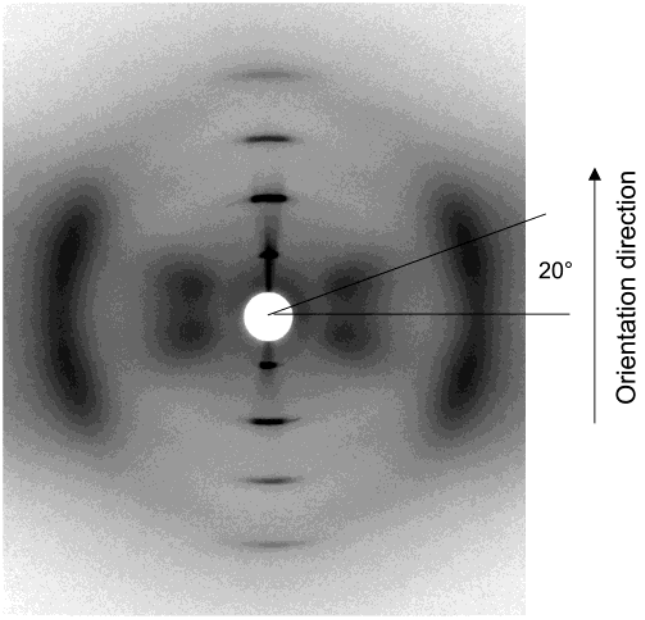

Figure 5. WAXD pattern of PDEGBB oriented at 65 °C after quenching and heat set at 155 °C for 6 h under tension.

arcs above and below the equator. These results indicated that the smectic layer normal was parallel to the orientation direction, and the mesogenic groups were tilted with respect to the orientation direction. The tilt angle measured directly from the splitting of the equatorial reflections was 20° to the layer normal, in good agreement with literature results.[31] Tilt of the mesogens differentiates the smectic CA form from the smectic A form, which has the mesogens oriented normal to the smectic plane. Not surprisingly, other LC poly(bibenzoates) with an odd number of carbon atoms in the spacer backbone take the smectic CA form.[23,30,32]

After slow cooling to 155 °C or annealing at 155 °C the layer reflection at 5.65° was more intense, and the second- and third-order reflections at 11.3° and 17.0° were more prominent; however, there was no change the layer spacing (Figure 4). It appeared that these thermal histories produced an LC glass with the same smectic CA structure as the quenched glass but with slightly better order. After crystallization the broad reflection at 20.5° split into at least two reflections with 2θ values of 19.8° and 20.7° (4.48 and 4.29 Å), and another broad reflection appeared at 27.2° (3.28 Å), indicating 3-dimensional crystalline order (Figure 4). However, there was only a small shift in the layer reflection from 5.65° to 5.60° (15.6 to 15.8 Å). A very small increase in trans fraction from 0.79 to 0.81, determined by the infrared method described previously,[24] confirmed that crystallization of PDEGBB did not require full chain extension.

Dynamic Mechanical Relaxations. Representative DMTA scans of PDEGBB films in Figure 6 show storage modulus (E') and loss tangent (tan δ) as a function of temperature. The β relaxation corresponds to the glass transition.[33,34] The peak temperature of 53 °C is in close agreement with literature reports.[33] The peak tan δ value was about 0.60 for the quenched LC glass, only about one-third the intensity of the tan δ peak for the glass transition of a typical non-LC amorphous glass. The accompanying drop in E' of 2 orders of magnitude was correspondingly less than the drop of 3−4 orders of magnitude observed with a non-LC glass. Slowly

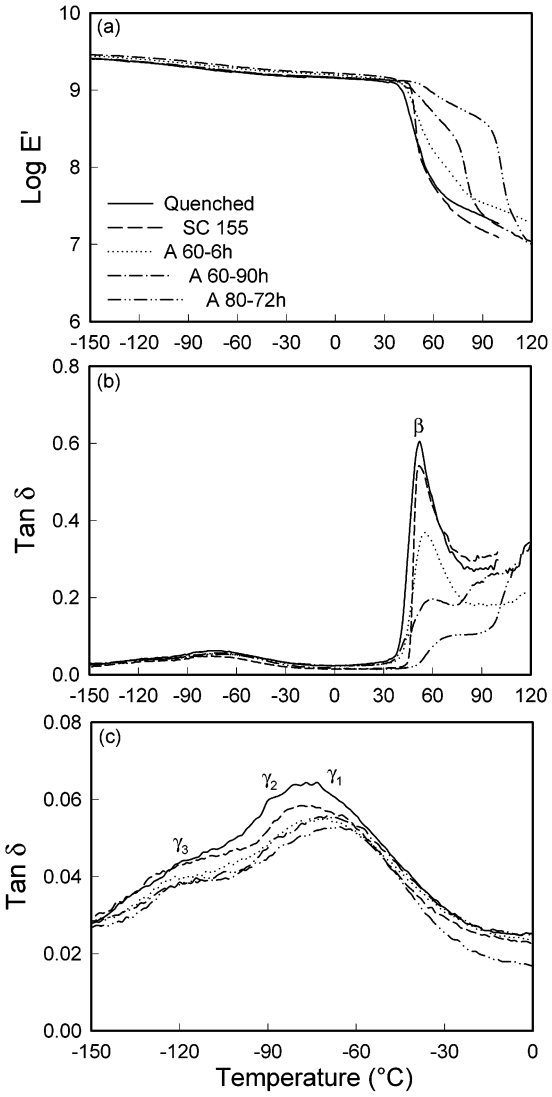

Figure 6. DMTA curves of quenched, slowly cooled and quenched, and then annealed PDEGBB: (a) log E'; (b) tan δ; (c) low-temperature range of tan δ.

cooling PDEGBB through the I−S transition produced only a slight decrease in tan δ peak intensity from 0.60 to 0.54 without affecting peak temperature, which suggested that the nature of the LC glass remained largely unchanged. In contrast, crystallization reduced the β-relaxation intensity considerably, broadened the peak, and increased the transition temperature (Figure 6). The accompanying drop in E' was correspondingly smaller. These effects followed trends that are typical for crystallization of a non-LC glass. Films with high crystallinity exhibited a second drop in E' at higher temperatures that was caused by the X−S transition.

The broad γ-relaxation from −150 to −30 °C is characteristic of aromatic polyesters with flexible spacers.[35−38] It is generally thought that the broad peak encompasses several relaxation processes involving spacer and ester linkages. The complexity of the γ-relaxation leads to identification of a higher temperature component (γ_1 at about −70 °C) with trans conformations of the spacer and a lower temperature component (γ_2 at about −100 °C) with gauche conformations of the spacer.[39,40] A slight shift of the γ-peak to higher temperature after crystallization (Figure 6c) was interpreted as an increase in intensity of the γ_1-relaxation

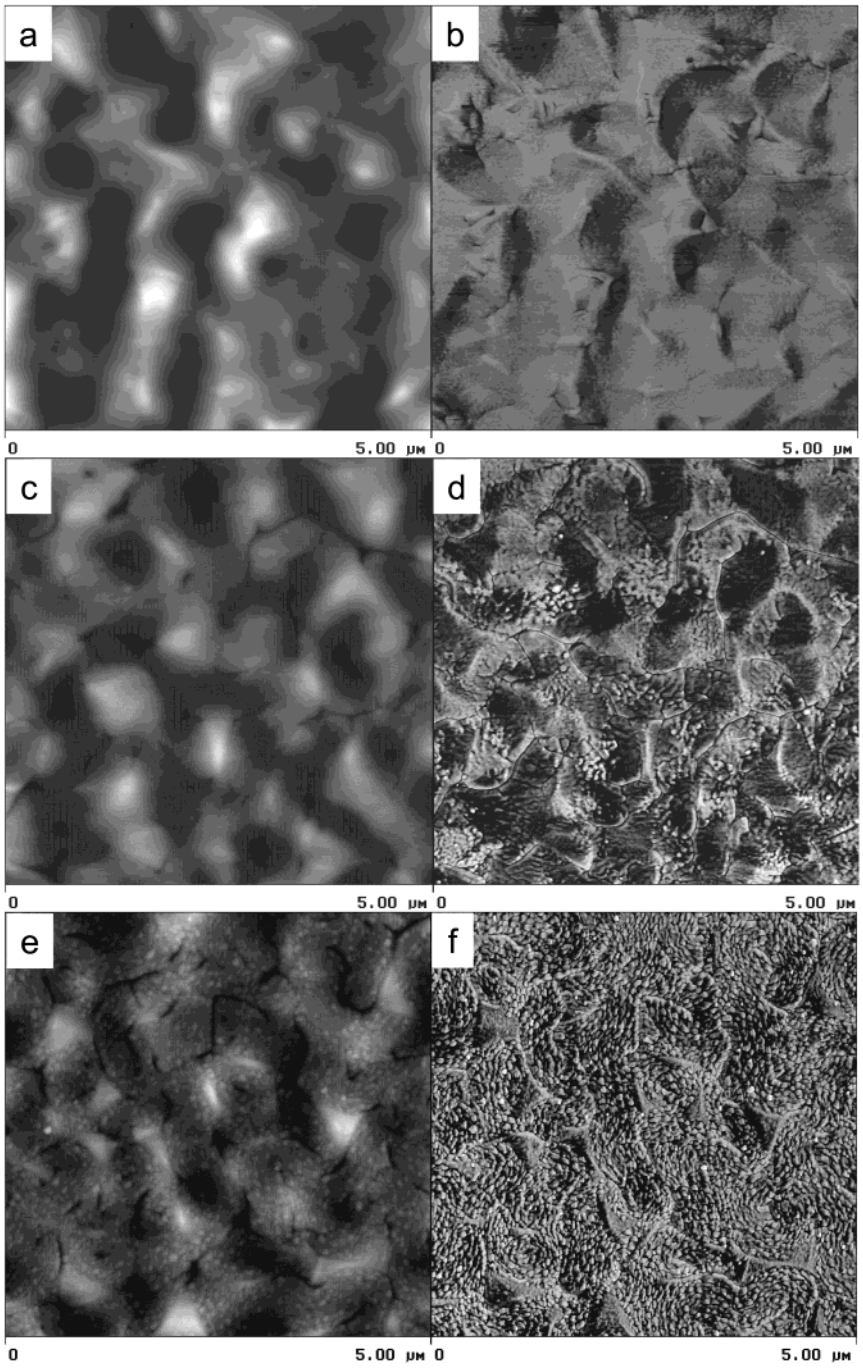

Figure 7. AFM images of slowly cooled PDEGBB: (a) and (b) height and phase images of the unetched surface; (c) and (d) height and phase images after 12 h etch; (e) and (f) height and phase images after 48 h etch.

relative to the γ_2-relaxation. This was consistent with the small increase in trans conformations from FTIR analysis. A third component of the γ-relaxation (γ_3 at about −120 °C) is associated with hindered motions of methylene groups and becomes stronger as the length of the spacer increases.[37,41] This relaxation showed no remarkable dependence on the thermal history (Figure 6).

Morphology. The morphology of the LC glass was probed with PDEGBB that had been slowly cooled through the I−S transition. Before etching, the surface displayed a polygonal texture in 5 μm AFM images in accordance with previous descriptions of smectic liquid crystals.[42] The polygonal domains were on the 2−3 μm size scale (Figure 7a,b). A relatively short etching time reduced the height of the polygonal topography and selectively removed the domain boundaries, making the domains clear in the AFM height image (Figure 7c). The corresponding phase image partially revealed the supermolecular texture within the domains (Figure 7d), which was more evident after longer etching (Figure 7e,f). The domains consisted of arrays of short lamellae with thickness of 70 nm. Such lamellar structures have frequently been reported in smectic and nematic LCPs.[43−46]

Quenching through the I−S transition prevented formation of well-defined polygonal domains on the surface of PDEGBB. However, etching revealed irregular boundaries of small, poorly defined domains on the size scale of 300−500 nm (Figure 8a). Individual lamellae were clearly distinguished in the corresponding phase image (Figure 8b). With thickness of about 50 nm

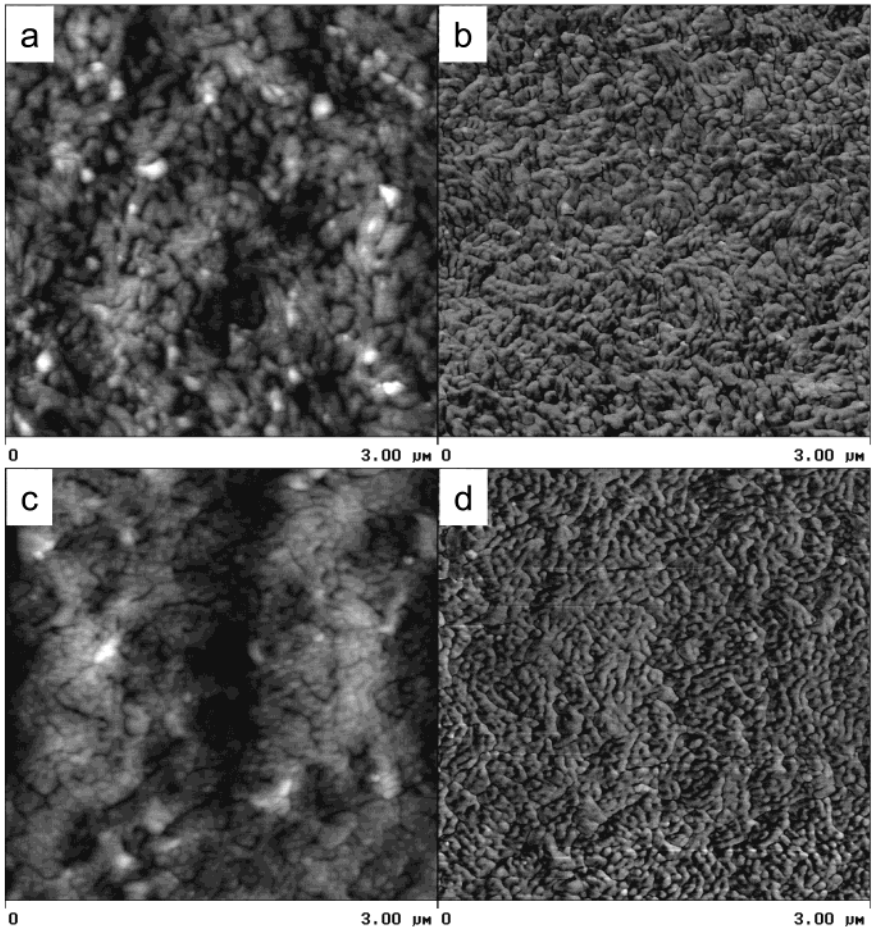

Figure 8. AFM images of quenched PDEGBB: (a) and (b) height and phase images of quenched PDEGBB after 48 h etch; (c) and (d) height and phase images of quenched PDEGBB annealed for 72 h at 80 °C after 48 h etch.

they were slightly thinner than the lamellae in slow-cooled films. Assemblies of a few aligned lamellae constituted poorly defined domains. After crystallization the domain boundaries were even less distinct (Figure 8c), and the lamellae were replaced with an overall granular texture (Figure 8d).

Structural Model. On the basis of the combined results of AFM and WAXD, it is possible to propose a hierarchical structural model for smectic PDEGBB. As depicted in Figure 9, the structural model closely resembles that proposed by Lipatov et al.[43] More or less extended chains assemble with the mesogens organized into smectic layers. From WAXD, the smectic layers are oriented perpendicular to the chain axis, and individual mesogens within the smectic layer are tilted at a slight angle to the chain direction. The spacing of the smectic layers is 1.56 nm from WAXD, which is less than the extended chain dimension, estimated at 1.82 nm. This may be a general feature of smectic LCPs and indicates some gauche kinks or eclipsed conformations. Stacks of smectic layers form lamellae. Regular stacking of the smectic layers is periodically interrupted by disordered regions that contain chain ends, chain folds, and other chain defects. These interruptions define the thickness of the lamellae, which is on the order of 70 nm. The lamellae often exhibit a granular texture that suggests some lateral variation in order within the regular stacking. Assemblies of lamellae define domains on the micron size scale. A domain in the liquid crystalline context is a region within which an orientation parameter varies slowly with position compared with its rapid variation or discontinuity at the delineating boundaries.[47] Disclinations produce the waviness in the lamellae, and groups of disclinations produce domain boundaries.[48]

Crystallization of PDEGBB does not produce lamellar or spherulitic features that are characteristic of non-LC aromatic polyesters.[49] Indeed, there appears to be no morphological manifestation of crystalline order in PDEGBB at the corresponding size scale. Additional crystalline order detected in other poly(bibenzoates) as a long spacing of 10−20 nm identifies a structural feature on a smaller size scale than the 70 nm lamellae.[50] If anything, LC order at the lamellar level is disrupted by crystallization to the extent that the lamellae become more granular in appearance. It is a general observation that crystallization from the LC state retains the texture of the LC precursor.[51−54] Because of the extended chain conformation in the smectic state, crystallization does not require axial shifts that would disrupt the smectic order, but rather only lateral translations and rotations about the chain axis. This is consistent with the frequently observed Avrami exponent close to 2 for crystallization from the LC or frustrated LC state, indicating a low dimensional growth.[49,51,53,55] Because it does not require large-scale structural rearrangements, crystallinity is attainable through transformation within the LC lamellae, leaving the domain structure largely undisturbed. Following previous studies of semicrystalline smectic LCPs, the structural image of crystallized PDEGBB consists of small fringed micellar crystals[56,57] imbedded in a smectic

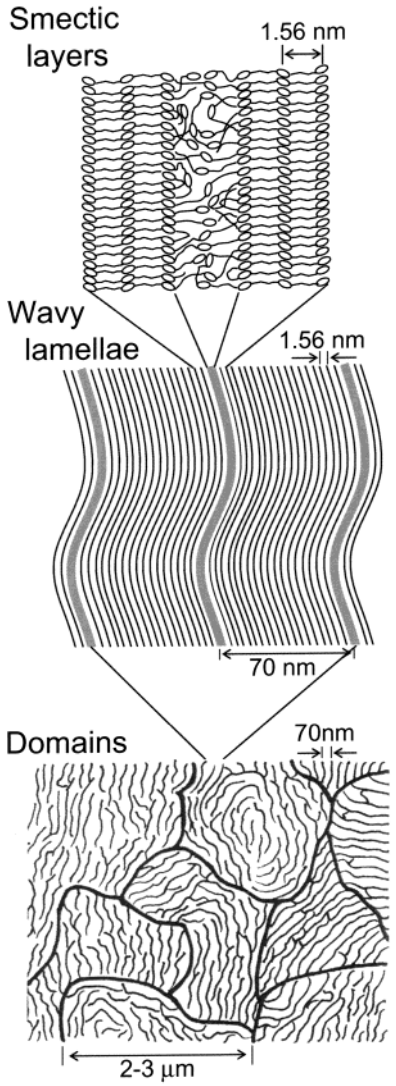

Figure 9. Hierarchical model of slowly cooled PDEGBB.

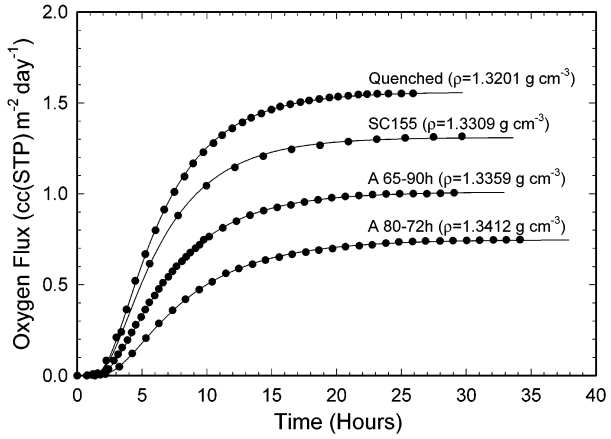

Figure 10. Experimental $J(t)$ data for PDEGBB films and the fit to eq 1.

mesophase which is not significantly disrupted by crystallization.[58,59]

Oxygen Transport. Typical experimental curves in Figure 10 describe the oxygen flux $J(t)$ through quenched, slow-cooled, and crystallized PDEGBB films. To facilitate comparisons among specimens that varied somewhat in thickness, the flux curves were normalized to a film thickness of 200 μm. Careful conditioning and appropriate choice of specimen thickness resulted in excellent resolution of the various features of the time dependence. The initial increase in oxygen flux reflected non-steady-state diffusion. This part of the curve was controlled mainly by the diffusivity D. As the permeant concentration in the specimen reached a constant distribution, the flux reached the steady-state value J_0. This value, normalized to the film thickness l and the permeant gas pressure p, defined the permeability $P = J_0 l p^{-1}$.

Compared to quenching, slow cooling did not affect the non-steady-state region of the flux curve whereas the steady-state flux decreased slightly (lower permeability). Crystallization of the quenched LC glass affected both the non-steady-state and steady-state parts of the flux curve. The non-steady-state region broadened slightly (lower diffusivity), and the steady-state flux decreased significantly. The fit to the solution of Fick's second law (eq 1) is included with the experimental points in Figure 10. The fit was equally good for all the experiments in the study. The two fitting parameters, P/l and D/l^2, were used to obtain diffusivity D and to accurately determine the permeability P. The solubility S was calculated from the relationship $S = PD^{-1}$.

Quenched PDEGBB had oxygen permeability more than 1 order of magnitude lower than that of amorphous poly(ethylene terephthalate) (PET) (Table 2). The permeability was comparable to that of another aromatic LC polyester with an aliphatic glycol, poly(ethylene terephthalate-*co*-*p*-hydroxybenzoate) (PET/HBA),[5] and an order of magnitude higher than permeability of a wholly aromatic LC polyester, poly(*p*-hydroxybenzoate-*co*-*p*-hydroxynaphthalate) (HBA/HNA).[8] The exceptionally low oxygen permeability of PDEGBB and other LCPs resulted mainly from very low gas solubility.

To better assess the effect of liquid crystallinity on transport characteristics, comparisons were made with a non-LC aromatic polyester having about the same T_g as PDEGBB, specifically with amorphous poly(trimethylene terephthalate) (PTT) with T_g of 41 °C. Oxygen permeability of PDEGBB was 0.0318 compared to 0.235 cm^3 (STP) cm m^{-2} day^{-1} atm^{-1} for PTT. The lower permeability of PDEGBB resulted in part from lower solubility, 0.0142 compared to 0.0463 cm^3 (STP) cm^{-3} atm^{-1} for PTT. A difference in oxygen diffusivity, 2.6×10^{-13} compared to 5.9×10^{-13} m^2 s^{-1} for PTT, also contributed to lower permeability of the LCP, although the effect of liquid crystallinity on D was not as large as that on S.

Crystallization of PDEGBB reduced oxygen transport as shown in Figure 11 with crystallinity expressed as density. Oxygen permeability decreased from 0.0318 to 0.0154 cm^3 (STP) cm m^{-2} day^{-1} atm^{-1} due to decreases in both D and S, with S decreasing more than D. The linear decrease in S with density extrapolated to $S = 0$ at a density of 1.371 g cm^{-3}. Increasing the density of the LC glass by slow cooling through the I−S transition, or annealing the quenched glass at a temperature just below the S−I transition, decreased S slightly without significantly affecting D (Table 1). The change in S conformed to the relationship between S and density as defined by crystallized PDEGBB in Figure 11.

Two-Phase Model for Oxygen Transport. Gas transport in crystalline non-LC polymers is often considered in terms of a two-phase model consisting of an impermeable crystalline phase dispersed in a permeable amorphous matrix. Thus, both sorption and diffusion

Table 2. Oxygen Barrier Properties of Selected Polyesters

samples		density (g cm^{-3})	T_g (°C)	crystallinity	P [cm^3 (STP) cm m^{-2} atm^{-1} day^{-1}]	D ($\times 10^{-13}$ m^2 s^{-1})	S [cm^3 (STP) cm^{-3} atm^{-1}]
PDEGBB	quenched	1.320	42		0.0318	2.6	0.0142
PET[a]	quenched	1.337	76	0.01	0.450	5.8	0.090
PTT	quenched	1.309	41	0.01	0.235	5.9	0.0463
PETBB55[b]	quenched	1.307	104	0.01	0.635	6.6	0.111
	melt-crystallized	1.343	90	0.39	0.158	2.6	0.070
	cold-crystallized	1.336	105	0.42	0.286	5.2	0.064
PET/HBA[c] (40/60)	solution cast	1.383	57.3	n/a	0.197	4.1	0.056
	solution cast and annealed	1.396	55.3	n/a	0.0281	3.2	0.010
HBA/HNA[d] (73/27)	as extruded	1.400	101	0.13	0.00386	0.97	0.0046
	annealed 0.2 h	1.399	103	0.19	0.00399	0.99	0.0044
	annealed 5 h	1.401	103	0.23	0.00316	0.79	0.0046
	annealed 24 h	1.404	107	0.26	0.00305	0.74	0.0048

[a] Reference 18; test temperature 25 °C. [b] Reference 20; melt-crystallized at 195 °C for 4.0 h; cold-crystallized at 115 °C for 4.0 h; test temperature 25 °C. [c] Reference 5; test temperature 35 °C; transport data were converted to 23 °C using the energetic parameters provided in ref 5. [d] Reference 8; annealing temperature 240 °C; test temperature 35 °C.

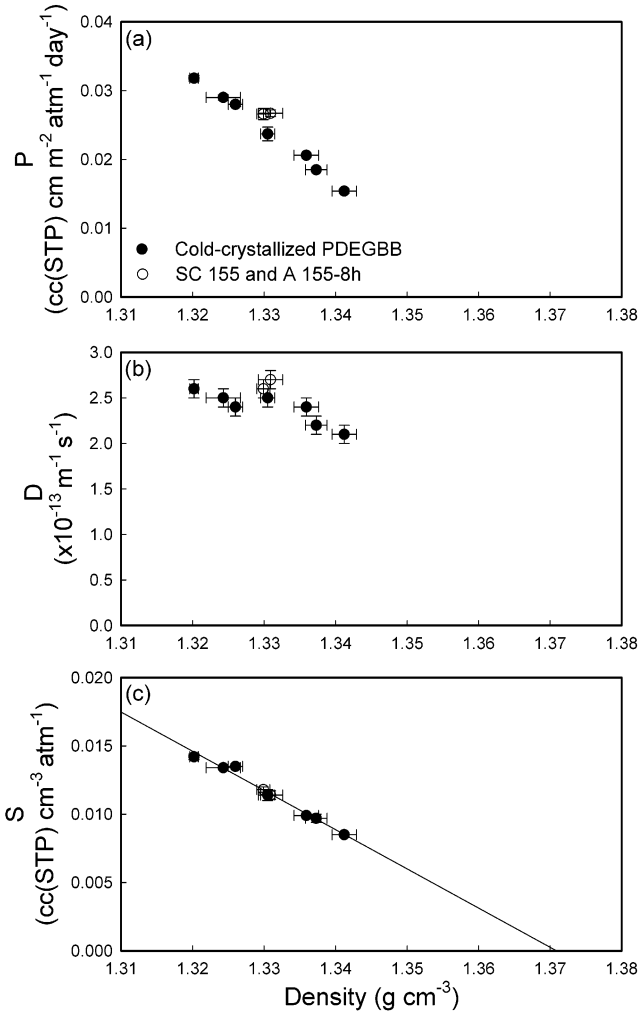

Figure 11. Effect of density on the oxygen transport parameters of PDEGBB: (a) permeability, (b) diffusivity, and (c) solubility.

are seen as taking place in the amorphous phase. The resulting relationship between solubility and crystallinity is

$$S = S_a(1 - \phi_c) \tag{2}$$

where S_a is the solubility of the gas in the amorphous phase and ϕ_c is the volume fraction crystallinity. If S_a is independent of the amount of crystallinity and equal to the solubility of the completely amorphous polymer, S will decrease linearly with volume fraction crystallinity and extrapolate to zero solubility at $\phi_c = 1$.

The linear relationship between S and crystallinity measured as density suggests that cold-crystallized PDEGBB also conforms to the two-phase model with

$$S = S_{LC}(1 - \phi_c) \tag{3}$$

where S_{LC} is the oxygen solubility of the quenched LC glass. It follows that volume fraction crystallinity ϕ_c can be calculated reliably from density ρ according to

$$\phi_c = \frac{\rho - \rho_{LC}}{\rho_c - \rho_{LC}} \tag{4}$$

where ρ_{LC} and ρ_c are the LC glass and crystal densities, respectively.

In applying eq 3 and eq 4 to PDEGBB, the crystal density cannot be obtained in the usual way from unit cell dimensions because the crystal structure is not available. Alternatively, the crystal density can be estimated by extrapolation to zero solubility, which gives $\rho_c = 1.371$ g cm^{-3}. An identical value (1.371 g cm^{-3}) is obtained for the crystal density by the group contribution method.[60] The extrapolated value also seems reasonable when compared with the reported crystal density of poly(ethylene 4,4′-bibenzoate)[61] of 1.426 g cm^{-3} and of poly(hexamethylene 4,4′-bibenzoate)[62] of 1.307 g cm^{-3}. The volume fraction crystallinity calculated from eq 4 is included in Table 1.

Extrapolation of the linear relationship between ΔH_{X-S} and density to 1.371 g cm^{-3} (Figure 3) provided $\Delta H°_{X-S} = 32.4$ J g^{-1} or 10.1 kJ mol^{-1}. One would expect a much higher $\Delta H°$ if the transition were from the crystal to the isotropic melt, estimated at 34 kJ mol^{-1} from group contributions.[63] However, others also found $\Delta H°$ for the crystal to LC transition to be relatively low.[58,64,65]

It is apparent from evidence presented here and elsewhere that very low gas solubility largely accounts for the exceptionally low gas permeability of LCPs compared to that of non-LC polymers. Two hypotheses have been put forward. One suggests that LC domains exclude permeant in the same way that most 3-dimensional crystals do, and transport is dominated by the small volume fraction of interdomain boundary regions. Alternatively, gas sorption occurs in the LC regions; however, ordered arrangement of the chains reduces gas

solubility to well below that of a conventional amorphous glass. Results for nematic HBA/HNA copolyesters appear to favor the first interpretation.[7,8] This conclusion is based primarily on the observation that increasing crystallinity as measured from melting enthalpy does not reduce gas solubility. However, in this example, crystallization also does not alter density, suggesting that density of the nematic phase is close to that of the crystal.[66,67] Taken together with the very small enthalpy change reported for the crystal-to-nematic transition of 3.7 kJ mol^{-1},[65] it appears that the nematic phase of HBA/HNA possesses a high level of order, close to that of the crystal, and can be considered almost impermeable. In support of this conclusion, it is noted that oxygen permeability of HBA/HNA is extremely low, an order of magnitude lower than that of PDEGBB (Table 2).

In contrast, the density of smectic PDEGBB is demonstratively less than the density of the crystal. Moreover, oxygen solubility decreases linearly with crystallinity as measured by density or melting enthalpy. This behavior is consistent with the second hypothesis as formulated in the two-phase transport model of impermeable crystallites dispersed in a permeable matrix, with the caveat that the LC matrix possesses much lower gas solubility than a conventional amorphous polymer.

The simple two-phase description of oxygen solubility was taken as the basis for examining diffusivity and permeability of cold-crystallized PDEGBB. The decrease in D with crystallinity arises from geometric impedance to the transport path imposed by impermeable 3-dimensional crystallites. The result can be dramatic if the effective aspect ratio of the crystallites is large. This occurs in polyesters that crystallize as lamellar crystals organized into spherulitic morphologies such as PET, PEN, and melt-crystallized PETBB55.[18−20] Compared to spherulitic polymers, the effect of crystallization on D of PDEGBB is quite modest despite the relatively high level of crystallinity inferred from changes in solubility and density. Crystallized PDEGBB differs from non-LC polyesters in not displaying features of lamellar or spherulitic crystallization. Rather, the structural image of crystallized PDEGBB is one of small crystallites embedded in liquid crystalline lamellae. Because of their low aspect ratio, the crystallites have a smaller effect than lamellar crystallites on D.

The concept of crystallized PDEGBB as small crystallites of low aspect ratio is modeled as a dispersion of impermeable particles in a permeable matrix. Numerous empirical expressions for permeability of such a dispersion are available, usually with the aspect ratio of the particle as an adjustable parameter. One approach is based on the generalized Maxwell model for gas transport in heterogeneous media. It gives the compositional dependence of permeability in a system of a less permeable phase dispersed in a higher permeability matrix as[68−70]

$$P = P_m\left[1 + \frac{\phi_d(1+G)}{\frac{(P_d/P_m)+G}{(P_d/P_m)-1} - \phi_d}\right] \qquad (5)$$

where subscripts d and m refer to dispersed phase and continuous phase, respectively, and ϕ_d is the volume fraction of dispersed phase. In this expression, G is a geometric factor that accounts for the shape of the dispersed phase. For isometric particles including spheres, $G = 2$. For the special case of a dispersion of impermeable particles, $P_d = 0$, and eq 5 for spheres reduces to

$$P = P_m\left[\frac{1-\phi_c}{1+{}^1/_2\phi_c}\right] \qquad (6)$$

where P_m is the permeability of the matrix. Applying eq 6 to crystallized PDEGBB, P_m is taken as the permeability of the quenched LC glass of 0.0318 cm^3 (STP) cm m^{-2} day^{-1} atm^{-1}, and ϕ_d is taken as the volume fraction crystallinity ϕ_c. The quantity P/P_m is plotted vs ϕ_c in Figure 12 with ϕ_c obtained from density according to eq 4. The solid line fit shows that eq 6 satisfactorily describes oxygen permeability of crystallized PDEGBB.

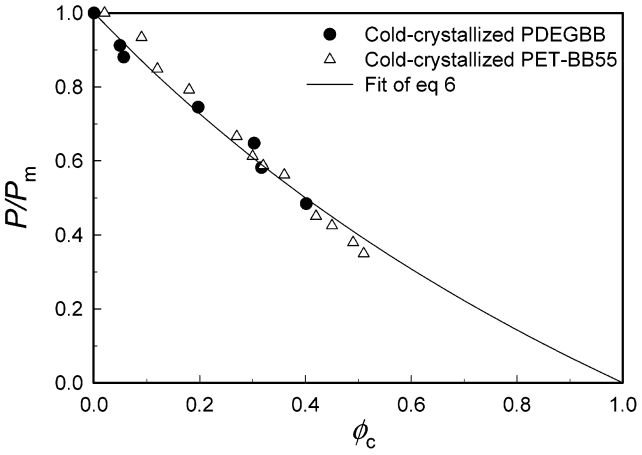

Figure 12. Relationship between the relative permeability (P/P_m) and ϕ_c for cold-crystallized PDEGBB and cold-crystallized PETBB55 (ref 20).

A granular morphology similar to that of cold-crystallized PDEGBB was previously observed in PETBB55 that was cold-crystallized from the glass. The PETBB55 copolymer is considered a "frustrated" LCP and is thought to take on liquid crystalline characteristics under certain conditions. As with PDEGBB, the granular morphology of cold-crystallized PETBB55 produces a relatively small effect on D, especially when compared with the effect of the more conventional spherulitic morphology obtained by crystallizing PETBB55 from the melt (Table 2). Results for oxygen permeability of cold-crystallized PETBB55 from the previous study are included in Figure 12. As formulated in eq 6, the Maxwell model for a dispersion of impermeable spheres also describes permeability of cold-crystallized PETBB55.

Conclusions

This study extends the two-phase transport model for oxygen transport of non-LC crystalline polymers to a smectic LCP. The challenges presented by the complex phase transitions and morphologies typical of LCPs are addressed by choosing an example from the well-characterized family of LC polyesters based on 4,4′-bibenzoic acid. It is possible to systematically vary the solid-state structure of poly(diethylene glycol bibenzoate) (PDEGBB) from LC glass to crystallized LC glass. The results are consistent with a liquid crystalline state intermediate between the permeable amorphous glass and the impermeable 3-dimensional crystal. In this interpretation, LC order naturally leads to inher-

ently low gas solubility. The results are not consistent with an LC phase that is impermeable to penetrant molecules. The hierarchical structure of the crystallized LC glass provides the basis for describing oxygen permeability in terms of the generalized Maxwell equation for spherical particles.

Acknowledgment. The authors thank Richard Y. F. Liu for providing the infrared determination of trans conformation fraction. Financial support from the National Science Foundation (DMR 9975774 and DMR 9986467) and KoSa is gratefully acknowledged. Modern Controls, Inc., generously supported the development of a facility for gas transport studies at Case Western Reserve University.

References and Notes

(1) Gorrasi, G.; Incarnato, L.; Di Maio, L.; Acierno, D.; Vittoria, V. *J. Macromol. Sci., Phys.* **1997**, *B36*, 643−653.
(2) Flodberg, G.; Hellman, A.; Hedenqvist, M. S.; Sadiku, E. R.; Gedde, U. W. *Polym. Eng. Sci.* **2000**, *40*, 1969−1978.
(3) Liu, R. Y. F.; Hu, Y. S.; Hibbs, M. R.; Collard, D. M.; Schiraldi, D. A.; Hiltner, A.; Baer, E. *J. Polym. Sci., Part B: Polym. Phys.* **2003**, *41*, 289−307.
(4) Chiou, J. S.; Paul, D. R. *J. Polym. Sci., Part B: Polym. Phys.* **1987**, *25*, 1699−1707.
(5) Weinkauf, D. H.; Paul, D. R. *J. Polym. Sci., Part B: Polym. Phys.* **1991**, *29*, 329−340.
(6) Weinkauf, D. H.; Paul, D. R. *J. Polym. Sci., Part B: Polym. Phys.* **1992**, *30*, 837−849.
(7) Weinkauf, D. H.; Paul, D. R. In *Barrier Polymers and Structures*; Koros, W. J., Ed.; American Chemical Society: Washington, DC, 1990; Chapter 3, pp 60−91.
(8) Weinkauf, D. H.; Paul, D. R. *J. Polym. Sci., Part B: Polym. Phys.* **1992**, *30*, 817−835.
(9) Chen, D.-S.; Hsiue, G.-H. *Polymer* **1994**, *35*, 2808−2814.
(10) Candia, F. D.; Renzulli, A.; Vittoria, V.; Roviello, A.; Sirigu, A. *J. Polym. Sci., Part B: Polym. Phys.* **1990**, *28*, 203−211.
(11) Cantrell, G. R.; Freeman, B. D.; Hopfenberg, H. B.; Makhija, S.; Haider, I.; Jaffe, M. In *Liquid Crystalline Polymers*; Carfagna, C., Ed.; Elsevier Science: Oxford, 1994; pp 233−251.
(12) Wunderlich, B.; Grebowicz, J. *Adv. Polym. Sci.* **1984**, *60/61*, 1−59.
(13) Monnerie, L. *Pure Appl. Chem.* **1985**, *57*, 1563−1588.
(14) Spiess, H. W. *Pure Appl. Chem.* **1985**, *57*, 1617−1626.
(15) Troughton, M. J.; Davies, G. R.; Ward, I. M. *Polymer* **1989**, *30*, 58−62.
(16) Frenzel, J.; Rehage, G. *Makromol. Chem. Rapid Commun.* **1980**, *1*, 129−134.
(17) Bahadur, B. *Mol. Cryst. Liq. Cryst.* **1976**, *35*, 83−99.
(18) Sekelik, D. J.; Stepanov, S. V.; Nazarenko, S.; Schiraldi, D.; Hiltner, A.; Baer, E. *J. Polym. Sci., Part B: Polym. Phys.* **1999**, *37*, 847−857.
(19) Hu, Y. S.; Liu, R. Y. F.; Zhang, L. Q.; Rogunova, M.; Schiraldi, D. A.; Nazarenko, S.; Hiltner, A.; Baer, E. *Macromolecules* **2002**, *35*, 7326−7337.
(20) Hu, Y. S.; Liu, R. Y. F.; Rogunova, M.; Schiraldi, D. A.; Nazarenko, S.; Hiltner, A.; Baer, E. *J. Polym. Sci., Part B: Polym. Phys.* **2002**, *40*, 2489−2503.
(21) Krigbaum, W. R.; Asrar, J.; Toriumi, H.; Ciferri, A.; Preston, J. *J. Polym. Sci., Polym. Lett. Ed.* **1982**, *20*, 109−115.
(22) Meurisse, P.; Noel, C.; Monnerie, L. Fayolle, B. *Br. Polym. J.* **1981**, *13*, 55−63.
(23) Watanabe, J.; Hayashi, M.; Nakata, T.; Niori, T.; Tokita, M. *Prog. Polym. Sci.* **1997**, *22*, 1053−1087.
(24) Hu, Y. S.; Liu, R. Y. F.; Schiraldi, D. A.; Hiltner, A.; Baer, E. *Macromolecules*, to be submitted.
(25) Organ, S. J.; Barham, P. J. *Polym. Prepr.* **1988**, *29*, 602.
(26) Tokita, M.; Osada, K.; Watanabe, J. *Polym. J.* **1998**, *30*, 589−595.
(27) Bello, A.; Riande, E.; Pérez, E.; Marugán, M. M.; Pereña, J. M. *Macromolecules* **1993**, *26*, 1072−1077.
(28) Abe, A. *Macromolecules* **1984**, *17*, 2280−2287.
(29) Watanabe, J.; Hayashi, M. *Macromolecules* **1988**, *21*, 278−280.
(30) Pérez, E.; Riande, E.; Bello, A.; Benavente, R.; Pereña, J. M. *Macromolecules* **1992**, *25*, 605−610.
(31) Tokita, M.; Osada, K.; Watanabe, J. *Liq. Cryst.* **1998**, *24*, 477−480.
(32) Watanabe, J.; Hayashi, M. *Macromolecules* **1989**, *22*, 4083−4088.
(33) Benavente, R.; Pereña, J. M.; Pérez, E.; Bello, A. *Polymer* **1993**, *34*, 2344−2347.
(34) Benavente, R.; Pereña, J. M.; Pérez, E.; Bello, A. *Polymer* **1994**, *35*, 3686−3690.
(35) Illers, K. H.; Breuer, H. *J. Colloid Sci.* **1963**, *18*, 1−31.
(36) Armeniades, C. D.; Baer, E. *J. Polym. Sci., Part A2* **1971**, *9*, 1345−1369.
(37) Yip, H. K.; Williams, H. L. *J. Appl. Polym. Sci.* **1976**, *20*, 1217−1230.
(38) Diaz-Calleja, R.; Riande, E.; Guzman, J. *Macromolecules* **1989**, *22*, 3654−3659.
(39) Hiltner, A.; Baer, E. *J. Macromol. Sci., Phys.* **1972**, *B6*, 545−558.
(40) Polyakova, A.; Connor, D. M.; Collard, D. M.; Schiraldi, D. A.; Hiltner, A.; Baer, E. *J. Polym. Sci., Part B: Polym. Phys.* **2001**, *39*, 1900−1910.
(41) Heaton, N. J.; Benavente, R.; Pérez, E.; Bello, A.; Pereña, J. M. *Polymer* **1996**, *37*, 3791−3798.
(42) Demus, D.; Richter, L. *Textures of Liquid Crystals*; VEB Deutscher Verlag für Grundstoffindustrie: Leipzig, 1978; Chapter 4, pp 27−101.
(43) Tsukruk, V. V.; Shilov, V. V.; Lipatov, Y. S. *Acta Polym.* **1985**, *36*, 403−412.
(44) Mazelet, G.; Kléman, M. *J. Mater. Sci.* **1988**, *23*, 3055−3060.
(45) Ford, J. R.; Bassett, D. C.; Mitchell, G. R. *Mol. Cryst. Liq. Cryst.* **1990**, *180B*, 233−243.
(46) Wang, W.; Lieser, G.; Wegner, G. *Macromolecules* **1994**, *27*, 1027−1032.
(47) General discussion: *Faraday Discuss. Chem. Soc.* **1985**, *79*, 175−190.
(48) Donald, A. M.; Windle, A. H. *Liquid Crystalline Polymers*; Cambridge University Press: Cambridge, 1992; Chapter 6, pp 169−199.
(49) Hu, Y. S.; Rogunova, M.; Schiraldi, D. A.; Hiltner, A.; Baer, E. *J. Appl. Polym. Sci.* **2002**, *86*, 98−115.
(50) Pérez, E.; Benavente, R.; Bello, A.; Pereña, J. M.; VanderHart, D. L. *Macromolecules* **1995**, *28*, 6211−6218.
(51) Warner, S. B.; Jaffe, M. *J. Cryst. Growth* **1980**, *48*, 184−190.
(52) Cheng, S. Z. D.; Yandrasits, M. A.; Percec, V. *Polymer* **1991**, *32*, 1284−1292.
(53) Pardey, R.; Zhang, A.; Gabori, P. A.; Harris, F. W.; Cheng, S. Z. D.; Adduci, J.; Facinelli, J. V.; Lenz, R. W. *Macromolecules* **1992**, *25*, 5060−5068.
(54) Heberer, D.; Keller, A.; Percec, V. *J. Polym. Sci., Part B: Polym. Phys.* **1995**, *33*, 1877−1894.
(55) Yandrasits, M. A.; Chen, J.; Arnold, F. E., Jr.; Cheng, S. Z. D.; Percec, V. *Polym. Adv. Technol.* **1994**, *5*, 775−784.
(56) Thomas, E. L.; Wood, B. A. *Faraday Discuss. Chem. Soc.* **1985**, *79*, 229−239.
(57) Butzbach, G. D.; Wendorff, J. H.; Zimmermann, H. J. *Polymer* **1986**, *27*, 1337−1344.
(58) Grebowicz, J.; Wunderlich, B. *J. Polym. Sci., Polym. Phys. Ed.* **1983**, *21*, 141−150.
(59) Hudson, S. D.; Lovinger, A. Z.; Gomez, M. A.; Jorente, J.; Marco, C.; Fatou, J. G. *Macromolecules* **1994**, *27*, 3357−3362.
(60) Van Krevelen, D. W. *Properties of Polymers*, 3rd ed.; Elsevier: Amsterdam, 1997; Chapter 4, pp 71−107.
(61) Li, X.; Brisse, F. *Macromolecules* **1994**, *27*, 2276−2282.
(62) Li, X.; Brisse, F. *Macromolecules* **1994**, *27*, 7725−7734.
(63) Van Krevelen, D. W. *Properties of Polymers*, 3rd ed.; Elsevier: Amsterdam, 1997; Chapter 5, pp 109−127.
(64) Campoy, I.; Marco, C.; Gómez, M. A.; Fatou, J. G. *Macromolecules* **1992**, *25*, 4392−4298.
(65) Cheng, S. Z. D. *Macromolecules* **1988**, *21*, 2475−2484.
(66) Butzbach, G. D.; Wendorff, J. H.; Zimmermann, H. J. *Makromol. Chem. Rapid Commun.* **1985**, *6*, 821−827.
(67) Hudson, S. D.; Lovinger, A. J. *Polymer* **1993**, *34*, 1123−1129.
(68) Petropoulos, J. H. *Adv. Polym. Sci.* **1985**, *64*, 93−142.
(69) Barrer, R. M. In *Diffusion in Polymers*; Crank, J., Park, G. S., Eds.; Academic: New York, 1968; Chapter 6, pp 165−217.
(70) Petropoulos, J. H. *J. Polym. Sci., Polym. Phys. Ed.* **1985**, *23*, 1309−1324.

MA0300746